The EMBO Journal (2007) 26, 3296–3307 | © 2007 European Molecular Biology Organization | All Rights Reserved 0261-4189/07
www.embojournal.org

THE EMBO JOURNAL

The *Caenorhabditis elegans* septin complex is nonpolar

Corinne M John[1,5,6], Richard K Hite[2,5], Christine S Weirich[1,5], Daniel J Fitzgerald[3,6], Hatim Jawhari[4,7], Mahamadou Faty[1,8], Dominik Schläpfer[1], Ruth Kroschewski[1], Fritz K Winkler[4], Tom Walz[2], Yves Barral[1,*] and Michel O Steinmetz[4]

[1]Institute of Biochemistry, ETH Zürich, Zürich, Switzerland, [2]Department of Cell Biology, Harvard Medical School, Boston, MA, USA, [3]Institute of Molecular Biology and Biophysics, ETH Zürich, Zürich, Switzerland and [4]Biomolecular Research, Structural Biology, Paul Scherrer Institut, Villigen, Switzerland

Septins are conserved GTPases that form heteromultimeric complexes and assemble into filaments that play a critical role in cell division and polarity. Results from budding and fission yeast indicate that septin complexes form around a tetrameric core. However, the molecular structure of the core and its influence on the polarity of septin complexes and filaments is poorly defined. The septin complex of the nematode *Caenorhabditis elegans* is formed entirely by the core septins UNC-59 and UNC-61. We show that UNC-59 and UNC-61 form a dimer of coiled-coil-mediated heterodimers. By electron microscopy, this heterotetramer appears as a linear arrangement of four densities representing the four septin subunits. Fusion of GFP to the N termini of UNC-59 and UNC-61 and subsequent electron microscopic visualization suggests that the sequence of septin subunits is UNC-59/UNC-61/UNC-61/UNC-59. Visualization of GFP extensions fused to the extremity of the C-terminal coiled coils indicates that these extend laterally from the heterotetrameric core. Together, our study establishes that the septin core complex is symmetric, and suggests that septins form nonpolar filaments.

The EMBO Journal (2007) **26,** 3296–3307. doi:10.1038/sj.emboj.7601775; Published online 28 June 2007
Subject Categories: cell & tissue architecture
Keywords: cell polarity; coiled coil; cytoskeleton; electron microscopy; septin

*Corresponding author. Institute of Biochemistry, ETH Zürich, 8093 Zürich, Switzerland. Tel.: +41 44 632 0678; Fax: +41 44 632 1591; E-mail: yves.barral@bc.biol.ethz.ch
[5]These authors contributed equally to this study
[6]Present address: Redbiotec AG, Wagistrasse 23, 8952 Schlieren, Switzerland
[7]Present address: Actelion Pharmaceuticals Ltd, Gewerbestrasse 16, 4123 Allschwil, Switzerland
[8]Present address: Friedrich-Miescher-Institute, WRO 1066-P46, Maulbeerstrasse 66, 4058 Basel, Switzerland

Received: 30 April 2007; accepted: 25 May 2007; published online: 28 June 2007

Introduction

The septins form a conserved family of GTPases found in fungi and animal cells (Kinoshita, 2003). During cell division, septins localize to sites of cytokinesis and are essential for this process in budding yeast, *Drosophila* embryos and mammalian tissue culture cells (Faty *et al*, 2002). In budding yeast, septins form a ring at the mother-bud neck composed of parallel arrays of filaments (Byers and Goetsch, 1976). This septin ring is closely associated with the plasma membrane and forms a scaffold to recruit myosin II and other cytokinetic factors to the future site of cleavage (Longtine and Bi, 2003). In addition, the septin ring contributes to the formation of a lateral diffusion barrier on the plasma membrane, which helps to maintain polarity factors in the bud (Barral *et al*, 2000; Takizawa *et al*, 2000). In metazoans, septins are also thought to be required for compartmentalization of the cell cortex (Schmidt and Nichols, 2004; Joo *et al*, 2005) and have been implicated in myriad cellular processes, including spindle assembly and orientation (Kusch *et al*, 2002; Spiliotis *et al*, 2005), exocytosis and vesicle trafficking (Hsu *et al*, 1998; Beites *et al*, 1999), cell migration (Finger *et al*, 2003), and apoptosis (Larisch *et al*, 2000; Gottfried *et al*, 2004). However, despite their important roles, the molecular properties of septins are poorly understood.

The septins share a common core consisting of a short N-terminal polybasic motif involved in phospholipid binding (Zhang *et al*, 1999), a central GTPase domain, a septin unique element/domain (SUE/SUD) of unknown function (Versele *et al*, 2004; Russell and Hall, 2005), and, in nearly all cases, a predicted coiled-coil domain at the C terminus (Versele *et al*, 2004). These proteins form hetero-oligomeric complexes, which are believed to be the basic repeating unit of the septin filament (Versele and Thorner, 2004). However, although the pairwise interactions between septin subunits have been identified (An *et al*, 2004; Versele *et al*, 2004; Low and Macara, 2006), the organization of monomers within the septin complex remains unclear. In particular, it is unclear whether the molecular arrangement within the core septin complex results in polar or nonpolar higher-order structures.

Data from budding yeast suggest that septins may form polar complexes. For example, the protein phosphatase regulator Bni4 localizes predominantly to the mother side of the septin ring (DeMarini *et al*, 1997; Kozubowski *et al*, 2003), whereas the septin-dependant kinase Hsl1 is found mainly on the daughter side (Barral *et al*, 1999). These observations suggest that the two faces of the septin ring offer different binding sites, and that septin filaments are therefore intrinsically polar. Alternatively, the asymmetric localization of these factors might reflect a septin-independent mechanism of polarity at the mother-bud neck.

The number of septins varies between organisms and cell types. For example, there are 7 septin genes in *Saccharomyces cerevisiae* (two of which function specifically in meiosis), 4 in *S. pombe*, and 13 in humans (Kinoshita *et al*, 2002; Sheffield

et al, 2003; An *et al*, 2004). One possibility is that the increased number of septins observed in mammalian cells reflects the increased functional variability of septin complexes in these organisms. Interestingly, despite the high degree of conservation between septins, they do not assume equivalent roles within the complex. In each case, a pair of septins forms a tetrameric core for the complex (Versele and Thorner, 2005). For example, only two of the five mitotic yeast septins, Cdc3 and Cdc12, are essential for vegetative growth, suggesting that they are crucial for septin complex assembly. Binding studies using recombinant proteins have shown that these subunits form the tetrameric core of the yeast septin complex (Versele *et al*, 2004; Farkasovsky *et al*, 2005). The closest *S. pombe* homologues of Cdc3 and Cdc12, Spn1, and Spn4, also form the heterotetrameric core of the fission yeast septin subunit (An *et al*, 2004). Similarly, the mammalian septins Sep2, Sep6, and Sep7 form a hexamer (Kinoshita *et al*, 2002; Sheffield *et al*, 2003) in which Sep6 and Sep7 are orthologous to Cdc3 and Cdc12. Thus, despite the variation observed among various septin complexes, the molecular organization of their core is a conserved heterotetramer.

The *Caenorhabditis elegans* genome encodes two septins, *unc-59* and *unc-61*. Both UNC-59 and UNC-61 have a predicted molecular weight (MW) of 52.9 kDa and share a common domain structure with low complexity regions predicted at the C terminus of UNC-59 and the N terminus of UNC-61 (Figure 1A; Versele and Thorner, 2005). The polybasic region, GTPase domain, and SUD domain of UNC-59 and UNC-61 have ~40% identity and ~60% similarity to each other. *In vivo*, both proteins are present at cleavage furrows and are essential for postembryonic cytokinesis and axon guidance (Nguyen *et al*, 2000; Finger *et al*, 2003). Furthermore, the presence of both molecules is required for their functions (Nguyen *et al*, 2000; Finger *et al*, 2003), suggesting that they act as an obligate heteromultimer. Thus, *C. elegans* septins, which are orthologous to Cdc3 and Cdc12, represent a minimal septin subunit and offer a powerful system to study the organization of core septin complexes.

In this paper, we have used a combination of cell biology, biochemistry, and electron microscopy (EM) to gain insight into the molecular organization of the UNC-59/UNC-61 septin complex. We show that UNC-59 and UNC-61 form a heterotetrameric complex capable of associating into higher-order structures in cells and filaments *in vitro*. In addition, we find that the C-terminal domains of UNC-59 and UNC-61 form parallel two-stranded coiled coils and that the heterotetrameric septin complex is assembled from UNC-59/UNC-61 heterodimers. EM studies show that the UNC-59/UNC-61 heterotetramer is an elongated, rod-like structure composed of two central UNC-61 subunits flanked by two UNC-59 subunits and that the UNC-59/UNC-61 coiled coils extend laterally from the heterotetramer. Together, our results delineate the molecular arrangement of monomers within the septin complex and suggest that septin complexes assemble into filaments and higher-order structures in a nonpolar fashion.

Results

C. elegans septins form higher-order structures in vivo

Although UNC-59 and UNC-61 have been shown to localize to the cleavage furrow in early embryos, it is not clear whether they assemble into filaments *in vivo* (Nguyen *et al*, 2000; Finger *et al*, 2003). To examine their ability to form filaments in cells, we investigated whether they polymerize when expressed in yeast and insect cells. Both septins localized diffusely throughout the cytoplasm and appeared at the bud neck in a small percentage of cells (8% of budded cells; Figure 1B and C). GFP-UNC-61 displayed similar localization and was present with slightly higher frequency at the bud neck (Figure 1B and C). In some cases, punctate structures were observed, which presumably corresponded to septin aggregates. When GFP-UNC-59 and UNC-61 were coexpressed, the number of yeast cells with a GFP-labeled bud neck increased to 73% (Figure 1B and C). In addition, filamentous structures stretching from the bud neck into the mother were frequently observed (Figure 1B). Together, these data indicate that both *C. elegans* septins incorporate into higher-order structures in cells, and that they form filamentous structures efficiently only when coexpressed. This is in agreement with the observation that UNC-59 and UNC-61 require each other for localization in the worm (Nguyen *et al*, 2000).

To determine whether UNC-59 and UNC-61 form complexes on their own or require endogenous septins, we investigated whether disruption of yeast septin complexes affected localization of the worm septins. The septin alleles *cdc12-1* and *cdc12-6* disrupt the assembly and stability, respectively, of yeast septin filaments at the restrictive temperature of 37°C (Dobbelaere *et al*, 2003). Cells carrying either mutation and expressing both GFP-UNC-59 and UNC-61 were shifted to the 37°C before visualizing GFP-UNC-59 by fluorescence microscopy (Figure 1D and data not shown). A strong GFP signal was still observed at the necks of these cells and in filamentous structures along the cell cortex. Thus, disruption of endogenous septin complexes did not affect the ability of UNC-59 and UNC-61 to assemble into filamentous structures. However, growth and morphological analyses indicated that coexpression of *C. elegans* septins was unable to complement the lack of endogenous septin structures. In addition, analysis of CFP-Cdc3 localization in *cdc12-6* cells coexpressing GFP-UNC-59 and UNC-61 at the restrictive temperature indicated that Cdc3 localization was not restored in these cells (Figure 1E). Together, these results suggest that coexpressed *C. elegans* septins assemble into filamentous structures that localize to the bud neck of yeast cells independently of endogenous septins.

Similar results were obtained when the two *C. elegans* septins were coexpressed in insect cells using baculovirus. Again, expression of UNC-59 or UNC-61 alone did not lead to filamentous structure formation (data not shown), whereas coexpression of both proteins did (Figure 1F). Together, these findings establish that UNC-59 and UNC-61 are necessary and sufficient to form higher-order structures in cells.

C. elegans septins form filaments in vitro

To understand complex formation by the *C. elegans* septins, we next expressed and purified UNC-59 and UNC-61 from *Escherichia coli* or insect cells. Neither UNC-61 nor UNC-59 was soluble when expressed alone (data not shown). In contrast, coexpression of UNC-59 and UNC-61 resulted in the production of a soluble complex from both bacteria and insect cells. 6 × His-UNC-59 and UNC-61 expressed in either

system co-eluted from a Ni-Sepharose column in a 1:1 ratio, indicating that they form a stochiometric complex (data not shown). These results are consistent with both *C. elegans* septins being required for proper localization (Figure 1B and C) and function (Nguyen *et al*, 2000).

Dialysis of purified yeast septins from high to low salt leads to assembly of long filaments (Frazier *et al*, 1998). We therefore tested the ability of bacterially produced UNC-59 and UNC-61 to form filaments under similar conditions. Affinity-purified septin complexes were subjected to

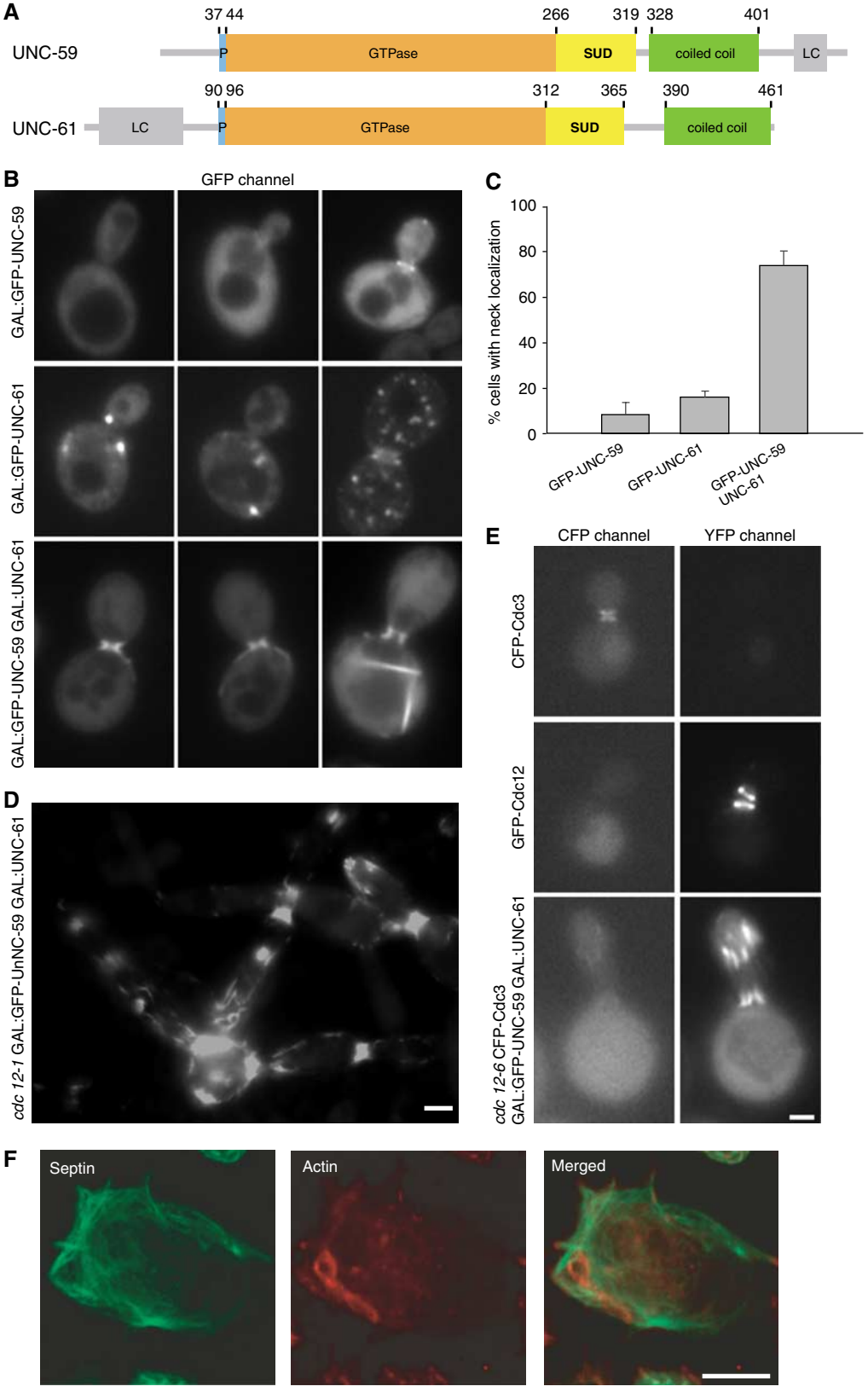

size-exclusion chromatography and the main peak fraction was isolated (see below). This fraction was dialyzed from 500 to 20 mM NaCl and filament formation was assessed by high-speed centrifugation and EM. Under these conditions, a few long and rigid filaments of up to 500 nm in length and 8–9 nm in width were observed (Figure 2A). Thus, bacterially expressed septins are able to polymerize *in vitro*, although with low efficiency.

When purified from insect cells, septin complexes assembled into filamentous sheets and bundles in 20 mM NaCl (Figure 2B and C). The number and thickness of these bundles increased, when dialysis was carried out at room temperature (Figure 2B and data not shown). Septin sheets and bundles often terminated in split endings. At these sites, the width of septin filaments measured either 8–9 or 16 nm (Figure 2C). These dimensions are similar to those of individual (7–9 nm) or pairs (14–18 nm) of yeast septin filaments (Frazier *et al*, 1998; Versele *et al*, 2004).

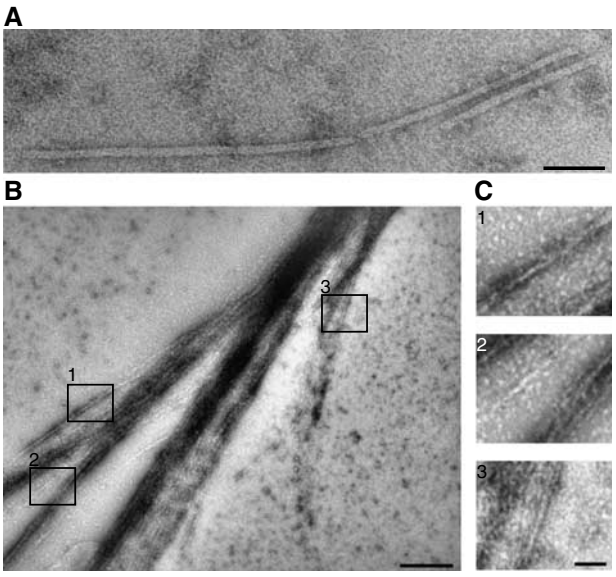

Figure 2 *C. elegans* septins form filaments *in vitro*. Electron micrographs of negatively stained septin filaments produced in *E. coli* (**A**) and insect cells (B, C) after dialysis from 500 mM NaCl into 20 mM NaCl buffer. (**B**) Overview of a septin filament sheet. (**C**) Enlargement of the indicated areas 1, 2, 3 from (B). The scale bar represents 50 nm in (A, C) and 250 nm in (B).

The C. elegans septin subunit is a dimer of UNC-59/UNC-61 heterodimers

To obtain a more detailed picture of the *C. elegans* septin subunit, we assessed nucleotide content and characterized the size and composition of recombinant UNC-59/UNC-61 complexes. In complexes purified from both *E. coli* and insect cells, low nucleotide content was observed; the ratio of GDP per septin monomer was <0.1 and no GTP was detected in any of the preparations (data not shown), suggesting that recombinant *C. elegans* septins were substoichiometrically loaded with nucleotide.

Next, we examined the size of the UNC-59/UNC-61 complex. Septins from both bacteria and insect cells eluted in three peaks over gel filtration (Figure 3A). The first peak corresponded to the void volume and contained aggregated septins. Based on the analysis of different fractions on protein gels and subsequent Coomassie staining, this aggregated material represented approximately 5% of septin prepared from *E. coli* (Figure 3B, lane 1). The second peak contained the largest fraction of the preparation (Figure 3B, lanes 2–4) and was further characterized by sedimentation velocity and equilibrium analytical ultracentrifugation (AUC). The average molecular mass of this fraction was 203 kDa with a sedimentation coefficient of 4S (data not shown), which corresponds to an elongated tetramer of UNC-59 and UNC-61. Based on static light scattering (SLS) analysis, the third peak in the size-exclusion chromatogram corresponds to a dimer (Figure 3B, lanes 5–7) with a molecular weight of 113 kDa. As UNC-59 and UNC-61 co-eluted from affinity- and size-exclusion chromatography at a 1:1 ratio, these results indicate that UNC-59 and UNC-61 contribute an equal number of subunits in both dimeric and tetrameric complexes.

To test the stability of the tetramer and dimer complexes, we analyzed these fractions by size-exclusion chromatography. The reapplied tetramer fraction remained primarily tetrameric, although a fraction dissociated into dimers (Figure 3D, black line). Molecular weights were determined by SLS to be 236 and 113 kDa, respectively. Similarly, the reapplied dimer fraction showed some tendency to associate into tetramers (Figure 3D, dashed black line). This tendency was enhanced upon four-fold concentration of the dimer fraction (Figure 3D, gray line).

C. elegans septins coexpressed in insect cells were also analyzed. $6\times$His-UNC-59 and UNC-61 co-eluted from a Ni-Sepharose column in a 1:1 ratio. Analysis of this complex by size-exclusion chromatography led to a similar chromatogram (Figure 3A, dotted line) with similar peak distribution and complex stability (Figure 3A and C). Together, these data indicate that septins produced in insect cells and bacteria behave similarly. In both cases, the heterotetrameric

Figure 1 Localization of *C. elegans* septins expressed in yeast and insect cells. (**A**) Schematic representation of the domain organization of the *C. elegans* septins UNC-59 and UNC-61. Both septins contain a polybasic region (P; blue), a GTPase domain (orange), a septin specific domain (SUD; yellow) and a predicted coiled-coil domain (green). The N- and the C-termini of UNC-61 and UNC-59, respectively, contain low complexity regions (LC; gray). Corresponding domain boundaries are indicated by residue positions. (B–E) Localization of *C. elegans* septins in *S. cerevisiae* as visualized by fluorescence microscopy. (**B**) WT yeast cells expressing the indicated combinations of GFP-tagged or untagged UNC-59 and UNC-61. (**C**) Quantification of budded cells showing septin localization at the bud neck where the indicated septin is expressed. (**D**) Typical localization of GFP-UNC-59 coexpressed with UNC-61 in the *cdc12–1* septin mutant upon overnight incubation at restrictive temperature. (**E**) Localization of CFP-Cdc3 and GFP-UNC-59 coexpressed with UNC-61 in *cdc12–6* cells after growth at 25°C overnight, followed by a 1 h shift to 37°C. As controls, WT yeast expressing either CFP-Cdc3 or GFP-Cdc12 was visualized in both YFP and CFP channels. (**F**) Visualization of *C. elegans* septins in SF21 insect cells by indirect immunofluorescence. SF21 cells expressing $6\times$His-UNC-59 and UNC-61 were stained with anti-penta-His antibodies (green) and filamentous actin was stained with rhodamin phalloidin (red). The scale bars represent 2 μm in (B, D, E) and 10 μm in (F).

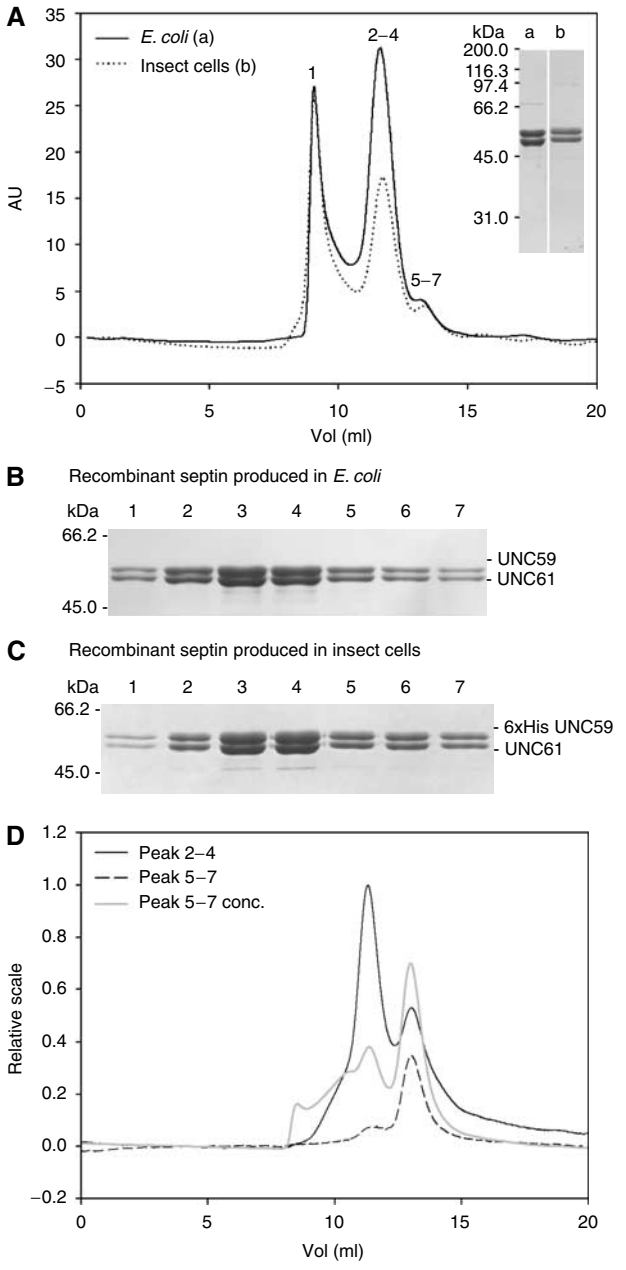

Figure 3 Analysis of the UNC-59/UNC-61 complex by size-exclusion chromatography. (**A**) Affinity-purified septin complex expressed in *E. coli* (solid line; 100 µl of 3 mg/ml injected) or in insect cells (dotted line; 100 µl of 1 mg/ml injected) was analyzed on a Superdex 200 column. Numbers on top of the peaks correspond to the lanes in the SDS–PAGE analysis (Coomassie stained) of septins produced in *E. coli* (**B**) or in insect cells (**C**). For SDS–PAGE comparison of septins (6 × His-UNC-59/UNC-61) produced in bacteria (a) or insect cells (b) see inset in (A). (**D**) Analysis of tetramer and dimer fractions. The tetramer fractions (2–4) (black line; 100 µl of 0.5 mg/ml injected), the dimer fractions (5–7) (black dashed line; 100 µl of 0.05 mg/ml injected) and a fourfold concentrated dimer fraction (gray line; 100 µl of 0.2 mg/ml injected) were rechromatographed on a Superdex 200 column.

complex, which resulted from dimerization of UNC-59/UNC-61 heterodimers, formed the main protein fraction. As the heterotetrameric complex is competent for polymerization (see above and Figure 2), it likely represents the basic building block of septin filaments.

C. elegans septin coiled coils form parallel heterodimers

To delineate the protein–protein interactions within the heterotetrameric septin complex, we next analyzed the role of the UNC-59 and UNC-61 coiled-coil domains. Both septins lacking their coiled-coil domains were insoluble when expressed alone and exhibited a strong tendency to precipitate when coexpressed (data not shown), suggesting that removal of these domains destabilize the proteins. We next investigated the homo- and heterotypic interactions of the coiled-coil domains of UNC-59 (residues 328-401, cc^{UNC-59}) and UNC-61 (residues 390-451, cc^{UNC-61}). At 5°C, cc^{UNC-59} (9.0 kDa) and cc^{UNC-61} (8.8 kDa) displayed far-ultraviolet (UV) CD spectra with minima at 205 and 222 nm (Figure 4A), characteristic of proteins with a helical content of 30–35%. Thermal unfolding experiments revealed broad transitions, indicating that the coiled-coil domains are largely denatured at 30°C (Figure 4A, inset). Sedimentation equilibrium experiments of cc^{UNC-59} and cc^{UNC-61} at 4°C yielded average molecular masses of 14 kDa in both cases, indicating an equilibrium between monomers and homodimers.

In contrast, the far-UV CD spectrum of a 1:1 mixture of cc^{UNC-59} and cc^{UNC-61} suggested a helical content of ~65% (Figure 4A). Thermal unfolding revealed a sigmoidal shaped melting profile with a midpoint of the transition, T_m, centered at 31°C (Figure 4A, inset). Both the CD spectrum and the melting profile are characteristic for moderately stable α-helical coiled-coil structures (Steinmetz *et al*, 1998). Sedimentation equilibrium AUC revealed an average molecular mass of 17 kDa, corresponding to a dimer of cc^{UNC-59} and cc^{UNC-61} (data not shown). Thus, cc^{UNC-59} and cc^{UNC-61} preferentially assemble into heterodimeric coiled-coil structures.

The relative orientation of cc^{UNC-59} and cc^{UNC-61} within the heterodimeric coiled coil was determined by fluorescence resonance energy transfer (FRET) and crosslinking experiments. For FRET experiments, cc^{UNC-59} was labeled at either the N or C terminus with BFP and tested for its ability to act as a FRET donor for cc^{UNC-61}-GFP. Combining cc^{UNC-59}-BFP and cc^{UNC-61}-GFP, but not BFP-cc^{UNC-59} and cc^{UNC-61}-GFP, resulted in energy transfer (Figure 4B), indicating that the septin coiled-coil domains engage in a parallel fashion. This interpretation was confirmed by cysteine crosslinking experiments (Harbury *et al*, 1993) in which the cc^{UNC-59} and cc^{UNC-61} constructs were engineered to contain an N-terminal cysteine, followed by two flexible glycines (CGGcc^{UNC-59} and CGGcc^{UNC-61}). These proteins were mixed in a 1:1 ratio and analyzed on reducing and nonreducing SDS–PAGE gels to separate monomers and disulfide bonded dimers (Figure 4C). Consistent with Cys-Cys disulfide-mediated crosslinking, dimers observed under nonreducing conditions were resolved into monomers under reducing conditions. In contrast, nearly no crosslinking was observed using cc^{UNC-59}GGC and CGGcc^{UNC-61} (data not shown). Together, these data show that cc^{UNC-59} and cc^{UNC-61} assemble into heterodimeric, parallel coiled coils.

The septin heterotetramer is an elongated UNC-59/UNC-61/UNC-61/UNC-59 complex

To understand its architecture, we visualized the UNC-59/UNC-61 heterotetramer using EM. Electron micrographs of negatively stained 6 × His-UNC-59/UNC-61 complexes derived from the tetrameric fraction (Figure 3A) showed elongated particles (Figure 5A). After image classification and

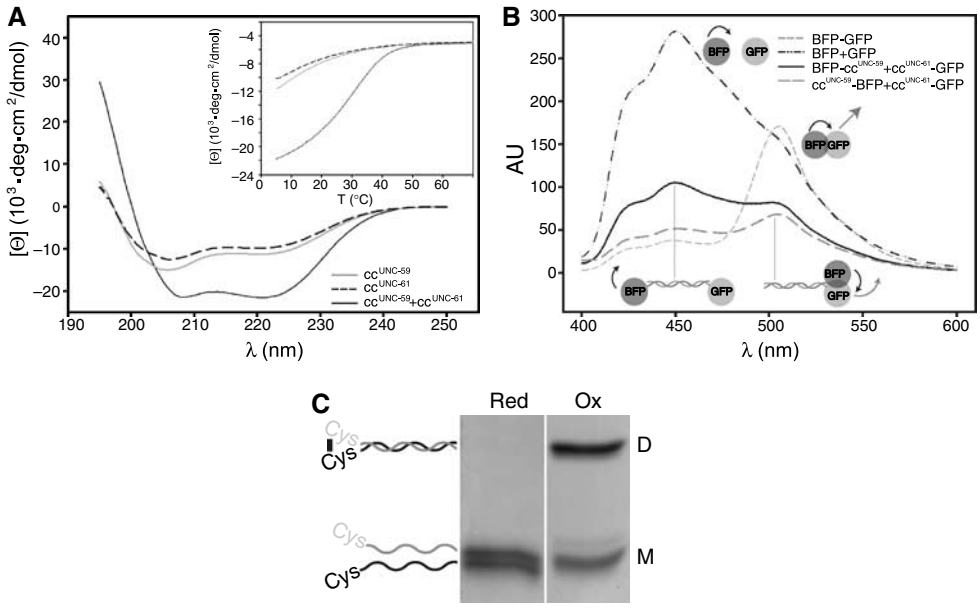

Figure 4 Analysis of the coiled-coil domains of UNC-59 and UNC-61. (**A**) Far-UV CD spectra of cc^{UNC-59} (gray line), cc^{UNC-61} (dashed line), and cc^{UNC-59} and cc^{UNC-61} mixed in equimolar ratio (solid line). (B, inset) Thermal unfolding profile recorded by CD at 222 nm. (B, C) Analysis of septin coiled-coil orientation. (**B**) FRET efficiency of soluble fractions of cells expressing cc^{UNC-59}BFP and cc^{UNC-61}GFP (solid line) or BFPcc^{UNC-59} and cc^{UNC-61}GFP (large dashed line), respectively. Positive control: BFP-GFP (small dashed line); negative control: BFP and GFP (dashed/dotted line). (**C**) Coomassie blue stained SDS–PAGE of CGGcc^{UNC-59} mixed in equimolar ratio with CGGcc^{UNC-61} under reducing (red) or oxidizing (ox) conditions. The migration positions of monomers (M) and dimers (D) are indicated schematically.

averaging, these particles appeared as four linearly arranged globular densities, each representing a subunit within the tetramer (Figure 5A, first eight panels). These particles are approximately 17–19 nm long and 5–7 nm wide, similar to the width of 7–9 nm measured for nematode (Figure 2), yeast and mammalian septin filaments (Field *et al*, 1996; Frazier *et al*, 1998; Kinoshita *et al*, 2002; Versele and Thorner, 2004). Panel 9 of Figure 5A shows a particle with only two densities, which most likely corresponds to the dimer observed by size-exclusion chromatography (Figure 3A and D). Together, these findings are consistent with the *C. elegans* septins forming a linear and stable UNC-59/UNC-61 heterotetrameric subunit.

To determine the positions of UNC-59 in the tetramer, an N-terminal GFP tag was fused to residues 23–459 of UNC-59. Affinity purified GFP-UNC-59 (23−459)/6 × HIS-UNC-61 behaved similarly to UNC-59/UNC-61, co-eluting during size-exclusion chromatography as a tetramer (data not shown). The GFP-labeled complexes were analyzed by EM (Figure 5B). Class averages revealed densities representing either or both of the GFP domains in addition to the four linear densities of the septin tetramer. Although several classes failed to resolve either of the GFP domains, in many of the class averages the position of at least one GFP was clearly discernable. To improve the signal-to-noise ratio of the averages, we selected 10 representative classes and used them as inputs for a second multireference alignment (Figure 5B, top row). The resulting class averages are very similar to the input images, but with clearer features (Figure 5B, middle row). In these averages, the GFP domain is localized to the terminal densities of the heterotetramer, suggesting that UNC-59 is located at the extremities of the septin complex.

To independently confirm this result, we decorated 6 × His-UNC-59/UNC-61 with Fab fragments directed against the 6 × His-tag at the N terminus of UNC-59 (Supplementary Figure 1). In decorated molecules, the Fab fragment was localized to one or both ends of the septin tetramer, consistent with the GFP-labeling experiment, indicating that UNC-59 localizes to the extremities of the heterotetramers.

We also identified the position of UNC-61 within the heterotetramer using GFP-labeling. To do this, we generated a construct containing an N-terminal GFP tag fused to UNC-61 residues 77–461. 6 × HIS-UNC-59/GFP-UNC-61 (77–461) co-eluted as a tetramer over gel filtration, suggesting that the predicted disordered region of UNC-61 is dispensable for tetramer formation. Purified 6 × HIS-UNC-59/GFP-UNC-61 (77–461) complexes were imaged by EM and particles were aligned using two rounds of multireference alignment as was performed for GFP-UNC-59 (23–459)/6 × HIS-UNC-61. The class averages that were used as the input references for a second multireference alignment are shown in Figure 5C, top row, and the resulting class averages are shown below (middle row). The GFP domain appears to be somewhat flexible. However, it is clearly localized to the central densities, placing the UNC-61 subunits at the center of the heterotetramer.

Taken together, our EM data strongly suggest that the heterotetramer corresponds to the tail-to-tail assembly of heterodimers into an elongated UNC-59/UNC-61/UNC-61/UNC-59 complex and thus is symmetric along its longitudinal axis.

The coiled coils extend laterally from the tetrameric septin core

To address the position of the coiled-coil domains in the heterotetrameric septin complex, we fused GFP to the C terminus of UNC-61, which corresponds to the extremity of the coiled-coil domain (Figure 1A). The GFP was

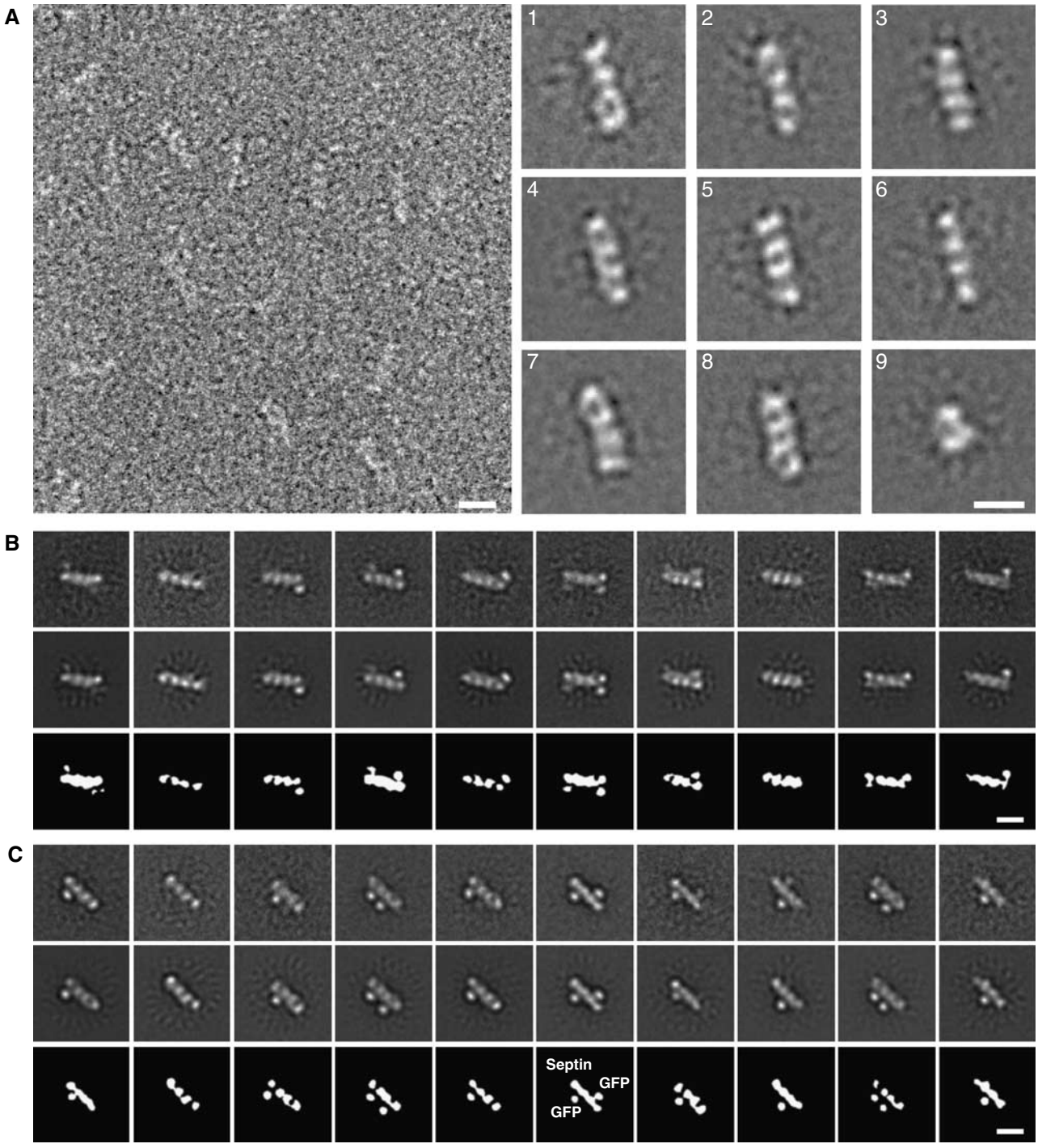

Figure 5 EM of septin complexes. (**A**) Electron micrograph and projection averages of negatively stained 6 × His-UNC-59/UNC-61 heterotetramers expressed in *E. coli*. The septin complexes stain poorly, making it difficult to see the linear septin molecules. The first eight panels show averages obtained from representative classes of septin heterotetramers containing four linearly arranged densities. The last panel is an average of heterodimers, which are composed of only two densities. (**B**) Projection averages of negatively stained GFP-UNC-59 (23–459)/6 × His-UNC-61 heterotetramers. The top panels show ten representative class averages from the multi-reference alignment using randomly selected raw images as initial references. These averages were used as input references for the second round of multi-reference alignment, whose outputs are shown in the middle row. Schematic diagrams of the averages from the second alignment are shown in the bottom row. (**C**) Projection averages of negatively stained 6 × His-UNC-59/GFP-UNC-61 (77–461) heterotetramers. The top panels show ten representative class averages from the multireference alignment using random references. These averages were used as input references for the second round of multireference alignment, whose outputs are shown in the middle row. Schematic diagrams of the averages from the second alignment are shown in the bottom row. All scale bars represent 10 nm.

introduced at the terminus of the coiled coil, because a two-stranded coiled coil does not have sufficient mass to be visualized by negative stain EM. Affinity-purified 6 × His-UNC-59/UNC-61-GFP behaved similarly to UNC-59/UNC-61 during size-exclusion chromatography, eluting primarily as a tetramer with a molecular weight of 256 kDa,

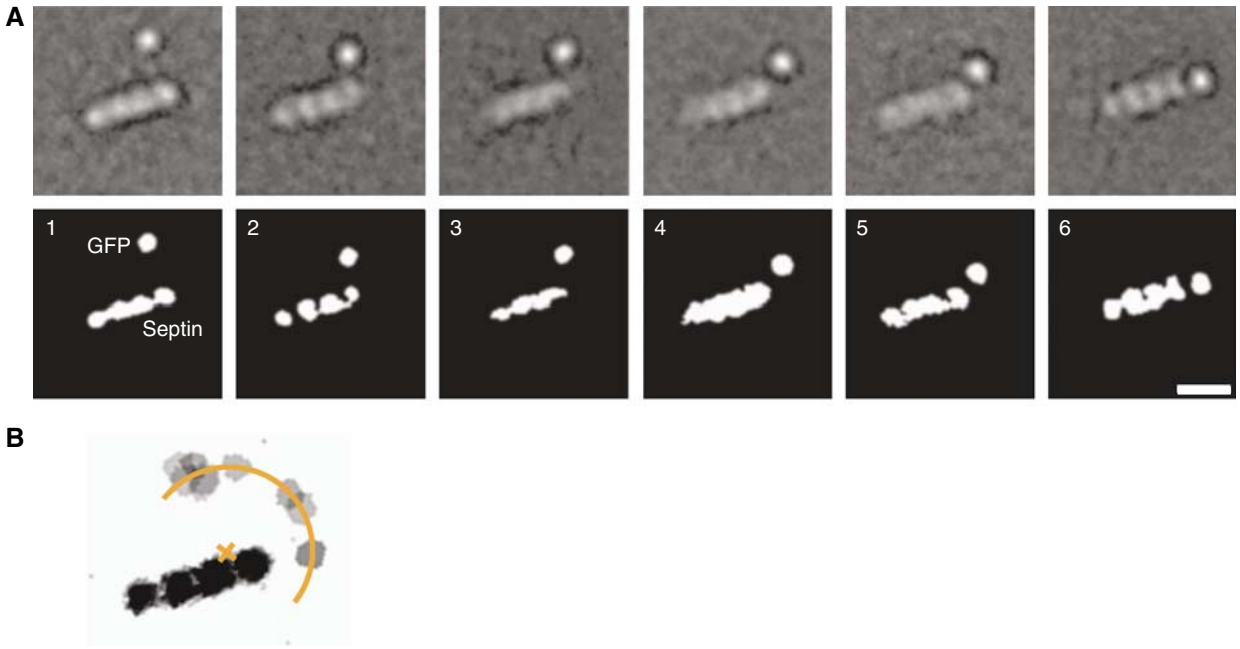

Figure 6 Flexibility of the coiled-coil domain. (**A**) Six representative class averages of UNC-59/UNC-61-GFP complexes showing one resolved GFP. The GFP is located at various positions relative to the heterotetramer core, demonstrating the flexibility of the coiled-coil/septin core junction. The scale bars represent 10 nm. (**B**) Schematic representation obtained by overlaying nine class averages of negatively stained 6 × His-UNC-59/UNC-61-GFP. Averages with the one resolved GFP moiety at the maximum distance from the four aligned globular domains were chosen. The coiled-coil domains occupy a semicircle around a heterodimer. The center lies at the interface between the UNC-59 and UNC-61 globular domains. The radius is about 10 nm.

as determined by SLS (data not shown). Visualization of this complex by EM revealed that the GFP density lies at a distance from the heterotetramer (Figure 6A). Due to this inherent structural variability, most averages resolved only one of the two GFPs, whereas the other one was averaged out. This implies that the two heterodimeric coiled coils extend laterally from the heterotetramer. Reminiscent to the 'thin strands' previously visualized by rotary metal shadowing EM (Hsu *et al*, 1998), the coiled-coil domains appear to radiate out from the septin heterotetramer at a variety of angles, resulting in the GFP moiety appearing in various positions relative to the heterotetramer core.

When we considered the averages in which the GFP moiety was located at the maximum distance from the four aligned globular densities, these GFPs formed an arc with a constant radius with respect to the center of either heterodimer core (Figure 6B). The radius of the GFP semicircle is 10 nm, which corresponds to the predicted length of the UNC-59/UNC-61 coiled coil. Thus, these data indicate that the heterodimeric coiled coil emanates from a point between the globular domains of the UNC-59/UNC-61 heterodimer and that the junction between the coiled-coil and globular domains is flexible.

Discussion

Critical aspects of the function and mechanism of a cellular cytoskeletal filament is directly related to the molecular organization of its core components. To date, the precise organization of the septin core structure has not been elucidated. To address this question, we investigated the structural organization of the *C. elegans* septins UNC-59 and UNC-61. Coexpression of UNC-59 and UNC-61 in *S. cerevisae*, insect cells or *E. coli* revealed that these two septins are necessary and sufficient for the formation of higher-order structures in cells and filaments *in vitro*, and are functionally similar to other, more complex septin assemblies (Field *et al*, 1996; Frazier *et al*, 1998; Kinoshita *et al*, 2002; Mendoza *et al*, 2002; Sheffield *et al*, 2003; Versele and Thorner, 2004). *In vivo*, these heterologous filaments formed and localized independently of endogenous septins. Thus, the *C. elegans* septins UNC-59 and UNC-61 represent an attractive minimal system to investigate the molecular structure of the septin core.

Our biochemical analysis revealed that the recombinantly expressed UNC-59 and UNC-61 are substoichiometrically loaded with guanine nucleotide (<0.1) and have no detectable GTP. This result is in contrast with studies of the *S. cerevisiae* septins showing that both endogenous and recombinant complexes are fully complexed with nucleotide and have a GDP:GTP ratio of 2.3:1 (Vrabioiu *et al*, 2004; Farkasovsky *et al*, 2005). This difference may be due to a limitation of our expression and purification methods or a species-specific difference between nematode and yeast septins. More specifically, because *C. elegans* has only two septin genes, it is possible that additional factors are required for full nucleotide binding by UNC-59 and UNC-61. In addition, although the role of GTP binding and hydrolysis remains unclear, it is likely to regulate some aspect of higher-order complex assembly. Thus, the lack of an additional factor may also explain the inefficient filament formation by UNC-59 and UNC-61 we observed (Figure 2).

However, our analysis establishes that UNC-59 and UNC-61 assemble into an obligate heterodimer that, in turn, assembles into a stable heterotetramer (Figure 3). Formation of the heterodimer required interactions between the parallel two-stranded coiled-coil domains of UNC-59 and UNC-61

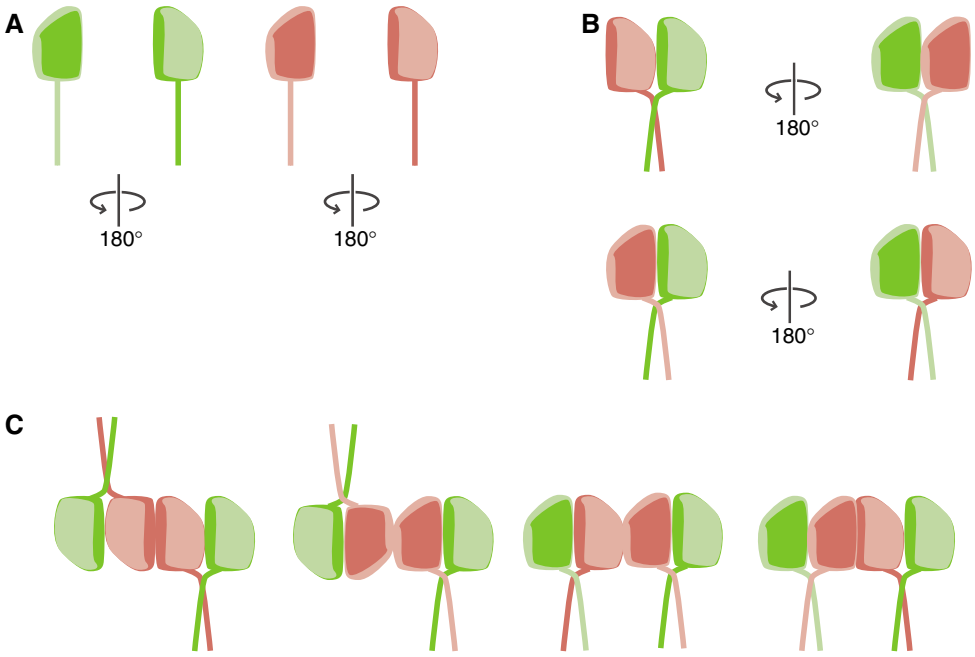

Figure 7 Molecular organization of the heterotetrameric septin core complex. (**A**) Schematic representations of UNC-59 (green) and UNC-61 (red), showing their GTPase domains and coiled-coil domains (rod). The GTPase domains are not internally symmetric, as represented by the 'top' face of the protein (arbitrary) shown as pale green or pink, and the 'bottom' side as dark green or red. (**B**) The septin heterodimer interacts via its globular domains and its parallel coiled coils. Diagrams show two possible modes of interaction between UNC-59 and UNC-61: 'top' to 'top', in which UNC-59 and UNC-61 are in the same orientation (top), and 'top' to 'bottom', in which they face opposite directions (bottom). (**C**) All models for heterotetramer formation require that two of three axes are nonpolar. Two of UNC-59/UNC-61 heterodimers dimerize along their longitudinal axis (X-axis). One two-fold symmetry axis between the two UNC-59/UNC-61 heterodimers is perpendicular to the drawing plane (Z-axis). Thus, the tetrameric septin subunit is nonpolar along X. In the first two models, the tetramer is also symmetric along the Y-axis, but asymmetric along the Z-axis. In the second two models, the tetramer is asymmetric along the y-axis, but symmetric along the Z-axis.

(Figures 4, 7A and B). These data are consistent with the finding that the hSep6/hSep7 and Cdc3/Cdc12 septin pairs, orthologs of the UNC-61/UNC-59 pair, interact via their coiled coils (Sheffield *et al*, 2003; Versele *et al*, 2004). UNC-61/UNC-59 heterodimers dimerize to form an elongated heterotetramer. Along the long axis of the core tetramer, subunit arrangements could result in a symmetric or asymmetric organization of heterodimers.

EM analysis of tetramers labeled with GFP on either the UNC-59 or UNC-61 subunits, as well as tetramers decorated with anti-His Fab fragments, indicated that the core septin tetramer is formed by homotypic interactions between UNC-61 subunits along its longitudinal axis, with a two-fold symmetry axis perpendicular to this (Figures 5B, C and 7C and Supplementary Figure 1). The width of the tetrameric subunit (5–7 nm) and the width of a single septin filament (8–9 nm) suggest that the subunits assemble along this longitudinal axis, presumably through UNC-59/UNC-59 interactions. As the two-fold axis of the *C. elegans* septin subunit is perpendicular to this direction, the resulting filament growth is nonpolar (Figure 7C). Although the coiled-coil domains were not visible in our EM preparations, we were able to visualize the extremity of the coiled coil using a GFP fusion. The resulting images indicated that the coiled coils are flexible around their point of origin and extend laterally from the heterotetramer core (Figure 6). If we assume that filament growth occurs by tetramer addition along the long axis of the core septin, then the coiled coils are available to make lateral contacts with other septin filaments in the context of septin bundles and sheets.

Parallel assemblies of septin filaments form sheets closely associated to the plasma membrane (Byers and Goetsch, 1976). Interestingly, our proposed model (Figure 7) results in an arrangement in which septin sheets have distinct polarities, consistent with data indicating that one face of the septin assembly engages the membrane, whereas the other face is exposed to the cytoplasm. Overall, we propose that, within a septin sheet, all axes within the plane of the sheet are nonpolar, but the axis perpendicular to the sheet is polar.

In conflict with this model, the asymmetric localization of Bni4 and Hsl1 to opposite sides of the septin ring has been proposed to depend on intrinsic septin polarity (Gladfelter *et al*, 2001). However, we have observed that mutants of Hsl1 that fail to interact with the septin ring localize in a polar manner in the cell and accumulate specifically at the bud cortex (Y. Barral, unpublished result), suggesting that Hsl1 polarity is not provided by intrinsic septin polarity, but rather by a septin-independent mechanism. This conclusion is supported by a recent study of Bni4 and Kcc4 in yeast, suggesting that the actin cytoskeleton is involved in the asymmetric distribution of these proteins (Kozubowski *et al*, 2005).

Our model of the septin core complex is compatible with genetic and proteomic data reported for the *S. cerevisiae* septin complex (Versele *et al*, 2004; Farkasovsky *et al*, 2005). The two essential septins Cdc3 and Cdc12 form a protease resistant tetrameric core within the nonameric yeast septin complex (Versele *et al*, 2004; Farkasovsky *et al*, 2005). However, the entire complex was proposed to be polar

(Versele *et al*, 2004; Farkasovsky *et al*, 2005). In light of our data, the orthologues of UNC-59 (Cdc12) and UNC-61 (Cdc3) are instead predicted to form a nonpolar tetrameric septin core: Cdc12-Cdc3-Cdc3-Cdc12, flanked by additional septin subunits. It is unclear how these peripheral septins would engage the tetrameric core, but one possibility is that the additional subunits would associate with the core at the extremities of the elongated tetramer. These models are supported by data on the dimensions of the septin complexes; the *C. elegans* septin core is 5–7 nm wide and 17–19 nm long (Figure 5), whereas the *S. cerevisae* complex has approximately the same width (7–9 nm), but is longer (32 nm) (Frazier *et al*, 1998), as would be expected if additional subunits are accommodated at each end.

Our results define the molecular organization of the tetrameric core of the septin complex, suggesting that septin filaments assemble in a nonpolar manner. Together, these findings provide a molecular basis for understanding of the formation and regulation of septin complexes. Importantly, these findings also suggest a mechanism for the formation of other higher-order septin structures containing polar surfaces, including sheets and gauzes.

Materials and methods

Yeast strain construction and fluorescence microscopy

All yeast media and standard genetic techniques were performed as described previously (Ausubel *et al*, 1987). All yeast strains were in the S288C background. For expression of *C. elegans* septins in yeast, the sequences encoding full-length *unc-59* and *unc-61* were cloned into the univector plasmid fusion system (Liu *et al*, 2000). *GFP-unc-59*, *GFP-unc-61*, and *loxH-unc-61* were expressed from a centromeric plasmid under the control of the *GAL1–10* promoter. Wild type (WT), *cdc12–1*, and *cdc12–6* yeast strains (Dobbelaere *et al*, 2003) were transformed with p*GFP-unc-59* (pFM250), p*GFP-unc-61*(pFM247), or p*GFP-unc-59* and *ploxH-unc-61* (pFM296). Fluorescence microscopy was carried out as described previously (Kusch *et al*, 2002).

For colocalization of endogenous CFP-Cdc3 with GFP-UNC-59 and UNC-61, *pGFP-unc-59* and ploxH-*unc-61* were transformed into either WT or *cdc12–6* strains containing *CFP-CDC3* integrated at the *URA3* locus (Dobbelaere *et al*, 2003). Expression of *unc-59* and *unc-61* was induced by growth on galactose plates overnight at 25°C. CFP- and GFP-labeled proteins were visualized using a BX50 microscope (Olympus) equipped with 425 nm and 504 nm filters and a monochromator (TILLphotonics) as a light source. As a control, WT strains expressing *GFP-CDC12* or *CFP-CDC3* and *cdc12–6* expressing *CFP-CDC3* were used. Pictures were taken with an IMAGO cooled CCD camera (TILLphotonics).

Insect cell culture

6 × His-unc-59 and *6 × His-unc-61* were coexpressed in SF21 insect cells using the Multibac baculovirus expression system (Berger *et al*, 2004). Protein purification, using a metal affinity column and size-exclusion chromatography, was performed exactly as for bacterially expressed protein (see below). The 6 × His-tag was not removed.

Immunofluorescence

At 72 h post-infection, insect cells were seeded on glass coverslips and processed for immunofluorescence essentially as described previously (Reinsch and Karsenti, 1994). Cells were labeled with penta-HIS antibody (dilution 1:150, Qiagen), followed by incubation with Alexa488-labeled secondary antibody (Molecular Probes) to visualize UNC-59 and UNC-61, and with Rhodamine-phalloidin (Molecular Probes) diluted in blocking solution to visualize filamentous actin. Pictures were acquired using confocal microscopy (LSM 510, Zeiss).

Construction of expression plasmids

For expression of full-length *unc-59* and *unc-61*, the sequences encoding amino acids 1–459 of *unc-59* and 1–462 of *unc-61* were PCR amplified from *C. elegans* cDNA clones yk465c12 or yk109f1, respectively (kind gift from Yuji Kohara, Genome Biology Lab, National Institute of Genetics, Mishima, Japan) and cloned into a pET15b (Novagen) derivative to generate plasmids pCJ37 (6 × His-*unc-59*), pCJ38 (6 × His-*unc-61*), and pCJ43 (6 × His-*unc-59* + *unc-61*). Sequences encoding the predicted coiled-coil domains of *unc-59* (residues 328–401) and *unc-61* (residues 390–451) were PCR amplified and cloned into vector pPEP-2 (Brandenberger *et al*, 1996), containing a 6 × His tag, fusion protein, and a thrombin cleavage site, to generate plasmids pCJ50 and pCJ51, respectively. The same sequences were inserted into vectors containing GFP and BFP (vectors kindly provided by I. Berger, Berger *et al*, 2003) to generate plasmids coexpressing cc^{UNC-59}-BFP and cc^{UNC-61}-GFP (pCJ68) and BFPcc^{UNC-59} and cc^{UNC-61}GFP (pCJ67).

To generate plasmid pCW156, the sequences encoding residues 1–461 of *unc-61* and GFP fused to residues 23–459 of *unc-59* were inserted into vector pDEST-PCA (kind gift of James Berger). Similarly, to generate plasmid pCW211, the sequences encoding residues 1–459 of *unc-59* and GFP fused to residues 77–461 of *unc-61* were inserted into the same vector.

Protein purification

The *E. coli* host strain JM109(DE3) (Promega) was used for expression. Bacterial cultures coexpressing either 6 × His-UNC-59/UNC-61 or 6 × His-UNC-59/UNC-61-GFP were induced at $A_{600} = 0.6$ with 1 mM IPTG for 5 h at 25°C. Purification was carried out on Ni^{2+}-Sepharose (GE Healthcare) under native conditions at 4°C as described in the manufacturer's instructions. Where indicated, the 6 × His-tag was removed. Proteins were dialyzed against high salt buffer (HSB: 20 mM HEPES 2 (pH 7.5), 500 mM NaCl, 1 mM DTT). After sedimentation (see below), the supernatant was applied to a Superdex 200 10/300 column (GE Healthcare). Peak fractions were collected, concentrated, and analyzed in downstream applications.

Bacterial cultures expressing the coiled coils were grown to $A_{600} = 0.6$ and induced with 1 mM IPTG for 5 h at 37°C. Metal affinity purification was carried out under denaturing conditions. The N-terminal tag was removed by thrombin cleavage.

For purification of GFP-UNC-59 (23–459)/6 × His-UNC-61 (1–462) and 6 × His-UNC-59 (1–459)/GFP-UNC-61 (77–462) complexes, cells were grown at 37°C to $A_{600} = 0.3$, shifted to 20°C, and induced with 0.25 mM IPTG for 12–16 h. After centrifugation, cells were resuspended in lysis buffer (50 mM HEPES (pH 7.5), 800 mM NaCl, 10% glycerol, 10 mM imidazole, 5 mM beta-mercaptomethanol, and 1 mM PMSF) and lysed by sonication. Complexes were purified using Ni-affinity chromatography (GE Healthcare), concentrated, and applied to a Superdex200 (10/300) in HSB.

Biochemical and biophysical characterization

Sedimentation experiments and filament preparation. Septin complexes from *E. coli* or insect cells (0.5–0.8 mg/ml) were dialyzed into low salt buffer (LSB: HSB with 20 mM NaCl) at 4 or 22°C for 12–16 h, then sedimented at 90 000 r.p.m. for 15 min at 4°C in a Beckman Optima TLX ultracentrifuge equipped with a TLA 100.1 rotor. Pellet and supernatant were analyzed by SDS–PAGE.

Nucleotide analysis. Nucleotide analysis using a C18 reversed-phase column was performed as described previously (Tucker *et al*, 1986). Alternatively, nucleotide was analyzed after protease treatment (Suter *et al*, 2006) with the following modifications: protein samples in buffer A (125 mM NaCl, 5 mM HEPES (pH 7.5), 0.25 mM DTT) were heated to 100°C for 5 min or treated with ProteinaseK for 30 min at 50°C before centrifugation using a table top centrifuge (Eppendorf) at 13 200 *g* for 5 min. GDP and GTP were separated and quantified on an anion exchange column (Nucleosil 4000–7 PEI, %0/4, Macherey-Nagel) with a linear gradient (0–1.5 M NaCl in 10 mM Tris–HCl, pH 8.0) using an HPLC system equipped with two independent UV-visible spectrometers (Shimadzu). Elution of samples was monitored at 259 nm.

Analytical ultracentrifugation. For AUC, UNC-59/UNC-61 was dialyzed into HSB; cc^{UNC-59} and cc^{UNC-61} were dialyzed into PBS. Measurements were carried out at a concentration of 0.5 mg/ml.

Analysis was performed as described previously (Fitzgerald *et al*, 2004). Equilibrium experiments were carried out at 9000, 12 000, and 14 000 r.p.m. for UNC-59/UNC-61 and at 40 000, 45 000 and 50 000 r.p.m. for cc^{UNC-59} and cc^{UNC-61}. Four individual sedimentation velocity experiments of UNC-59/UNC-61 were carried out at 30 000 r.p.m. under identical solution conditions as the equilibrium measurements.

Static light scattering. SLS experiments were performed using a miniDAWN TriStar with Optilab rex refractometer (Wyatt) coupled to a Superdex 200 10/30 gel filtration column on an Agilent 1100 Series HPLC. Molecular masses were calculated using the Wyatt Astra version 4.90.08 software package.

Circular dichroism spectroscopy. For CD spectroscopy, protein samples were in PBS. Far-UV CD spectra and thermal unfolding profiles were recorded on a J-810 spectropolarimeter (Jasco Inc.) as described previously (Honnappa *et al*, 2005).

Coiled coil orientation. FRET experiments were carried out as described previously (Berger *et al*, 2003; Philipps *et al*, 2003). Clarified cell extracts in PBS containing cc^{UNC-59}-BFP and cc^{UNC-61}-GFP or BFP-cc^{UNC-59} and cc^{UNC-61}-GFP were normalized to similar levels of GFP emission, and analyzed for FRET efficiency. Cysteine crosslinking experiments were carried out as described previously (Harbury *et al*, 1993). CGG septin coiled-coil combinations (CGG-cc^{UNC-59} with CGG-cc^{UNC-61} or cc^{UNC-59}-CGG with CGG-cc^{UNC-61}) in 8 M urea were dialyzed into PBS buffer and analyzed by SDS–PAGE under reducing and nonreducing conditions.

Electron microscopy and image processing. Septin filaments were adsorbed on glow discharged, carbon coated copper grids, and negatively stained with 2% uranyl acetate. Electron micrographs were obtained using a Philips Morgagni Transmission Electron Microscope operated at 80 kV, which was equipped with a Megaview III CCD camera.

Septin tetramers (3 µl, 0.05–0.1 mg/ml) were applied to glow discharged carbon-coated copper grids, washed in two drops of deionized water and stained in two drops of 0.75% uranyl formate (Ohi *et al*, 2004). Imaging was performed with a FEI Tecnai T12 electron microscope operating at an acceleration voltage of 120 kV. Images were taken at $\times$ 52 000 at a defocus of -2 µm using low-dose procedures on Kodak SO-163 film. Films were developed for 12 min with full-strength Kodak D-19 developer at 20°C. Films were digitized using a Zeiss SCAI scanner using a step size of 7 µm, and 3×3 pixels were binned to produce a pixel size of 4.04 Å.

For native septins, 12 957 particles were manually selected from 32 images using WEB, the display program associated with the image processing package SPIDER (Frank *et al*, 1996), which was used for all further image processing steps. Selected particles were windowed into 100×100 pixel images. Particles were normalized against the background and then subjected to eight rounds of multireference alignment. Each round of multireference alignment was followed by principal component analysis and K-means classification specifying 100 output classes. The references used for the first round of alignment were randomly chosen from the raw images. Nine representative images of the class averages are shown in Figure 5A.

For the GFP-UNC-59 (23–459)/6 $\times$ HIS-UNC61 (1–461) complex, 8802 particles were manually selected from 56 images. For the 6 $\times$ HIS-UNC-59 (1–459)/GFP-UNC61 (77–461) complex, 7883 particles were selected from 112 images. Particles were windowed into 100×100 pixel images and classified into 100 classes as described above. An additional multireference alignment step was added. Ten representative class averages from the final round of the initial multireference alignment were chosen and used as initial models for a second iteration of 10 rounds of multireference alignment. Each round of the alignment was followed by principal component analysis and K-means classification into 10 output classes. The input (top row) and output (middle row) classes of the GFP-UNC-59 (23–459)/6 $\times$ HIS-UNC61 (1–461) complexes are shown in Figure 5B and of the 6 $\times$ HIS-UNC-59 (1–459)/GFP-UNC61 (77–461) complexes in Figure 5C.

For UNC-59 (1–459)/UNC-61 (1–461)-GFP complexes, 11 092 particles were selected from 59 images, windowed into 100×100 pixel images and classified into 200 classes as described above. Six representative classes in which one GFP was resolved are presented in Figure 6A.

The α-His Fab fragment was prepared from an α-His antibody (Serotech) using the ImmunoPure® IgG1 Fab preparation kit (Pierce Biotechnology), according to the manufacturer's instructions. Fab-Septin complexes were formed by incubating 6 $\times$ His-UNC-59/UNC-61 with Fab fragments at a molar ratio of 1:4 and 1:8 (single Fab-labeled) or 1:20 (double Fab-labeled) overnight at 4°C in 20 mM HEPES (pH 7.5), 500 mM NaCl, 1 mM DTT (Nakagawa *et al*, 2005). For the Fab-labeled septins, 1189 singly labeled particles were selected from 41 images, windowed into 100×100 pixel images, classified into 20 classes to produce the representative class average shown in Supplementary Figure 1 (panel 1). A total of 364 doubly labeled particles were initially selected from 167 images and windowed into 100×100 pixel images. Due to the heterogeneity and poor contrast of the raw images, only the very best 42 particles were selected and classified into four classes using the procedure described. The resulting class average of the doubly labeled molecules is shown in Supplementary Figure 1 (panel 4).

Supplementary data

Supplementary data are available at *The EMBO Journal* Online (http://www.embojournal.org).

Acknowledgements

We thank I Berger, J Dobbelaere, Y Kohara, and J Berger for strains and reagents. We are grateful to S Honnapa for assistance with CD experiments, B Maco, H Gross and P Tittman for assistance with EM, C Norden for assistance with fluorescence microscopy, and JP Erzberger for assistance with construct design, protein purification, and manuscript preparation. The molecular EM facility at Harvard Medical School was established with a generous donation from the Giovanni Armenise Harvard Center for Structural Biology and is maintained with funds from NIH grant GM62580 (to TW). This work was supported by the Swiss National Science Foundation, within the framework of the National Center of Competence in Research Structural Biology program, and ETH funding. RKH is supported by NIH training grant 5T32HD007390. CSW is an EMBO fellow. YB is an EMBO young investigator.

References

An H, Morrell JL, Jennings JL, Link AJ, Gould KL (2004) Requirements of fission yeast septins for complex formation, localization, and function. *Mol Biol Cell* **15:** 5551–5564

Ausubel FM, Brent R, Kingston RE, Moore DD, Seidman JG, Smth JA, Struhl K (eds). (1987) *Current Protocols in Molecular Biology.* Harvard Medical School, Boston: John Wiley and Sons

Barral Y, Mermall V, Mooseker MS, Snyder M (2000) Compartmentalization of the cell cortex by septins is required for maintenance of cell polarity in yeast. *Mol Cell* **5:** 841–851

Barral Y, Parra M, Bidlingmaier S, Snyder M (1999) Nim1-related kinases coordinate cell cycle progression with the organization of the peripheral cytoskeleton in yeast. *Genes Dev* **13:** 176–187

Beites CL, Xie H, Bowser R, Trimble WS (1999) The septin CDCrel-1 binds syntaxin and inhibits exocytosis. *Nat Neurosci* **2:** 434–439

Berger I, Fitzgerald DJ, Richmond TJ (2004) Baculovirus expression system for heterologous multiprotein complexes. *Nat Biotechnol* **22:** 1583–1587

Berger P, Schaffitzel C, Berger I, Ban N, Suter U (2003) Membrane association of myotubularin-related protein 2 is mediated by a pleckstrin homology-GRAM domain and a coiled-coil dimerization module. *Proc Natl Acad Sci USA* **100:** 12177–12182

Brandenberger R, Kammerer RA, Engel J, Chiquet M (1996) Native chick laminin-4 containing the beta 2 chain (s-laminin) promotes motor axon growth. *J Cell Biol* **135:** 1583–1592

Byers B, Goetsch L (1976) A highly ordered ring of membrane-associated filaments in budding yeast. *J Cell Biol* **69:** 717–721

DeMarini DJ, Adams AE, Fares H, De Virgilio C, Valle G, Chuang JS, Pringle JR (1997) A septin-based hierarchy of proteins required

for localized deposition of chitin in the *Saccharomyces cerevisiae* cell wall. *J Cell Biol* **139:** 75–93
Dobbelaere J, Gentry MS, Hallberg RL, Barral Y (2003) Phosphorylation-dependent regulation of septin dynamics during the cell cycle. *Dev Cell* **4:** 345–357
Farkasovsky M, Herter P, Voss B, Wittinghofer A (2005) Nucleotide binding and filament assembly of recombinant yeast septin complexes. *Biol Chem* **386:** 643–656
Faty M, Fink M, Barral Y (2002) Septins: a ring to part mother and daughter. *Curr Genet* **41:** 123–131
Field CM, al-Awar O, Rosenblatt J, Wong ML, Alberts B, Mitchison TJ (1996) A purified *Drosophila* septin complex forms filaments and exhibits GTPase activity. *J Cell Biol* **133:** 605–616
Finger FP, Kopish KR, White JG (2003) A role for septins in cellular and axonal migration in *C. elegans*. *Dev Biol* **261:** 220–234
Fitzgerald DJ, DeLuca C, Berger I, Gaillard H, Sigrist R, Schimmele K, Richmond TJ (2004) Reaction cycle of the yeast Isw2 chromatin remodeling complex. *EMBO J* **23:** 3836–3843
Frank J, Radermacher M, Penczek P, Zhu J, Li Y, Ladjadj M, Leith A (1996) SPIDER and WEB: processing and visualization of images in 3D electron microscopy and related fields. *J Struct Biol* **116:** 190–199
Frazier JA, Wong ML, Longtine MS, Pringle JR, Mann M, Mitchison TJ, Field C (1998) Polymerization of purified yeast septins: evidence that organized filament arrays may not be required for septin function. *J Cell Biol* **143:** 737–749
Gladfelter AS, Pringle JR, Lew DJ (2001) The septin cortex at the yeast mother-bud neck. *Curr Opin Microbiol* **4:** 681–689
Gottfried Y, Rotem A, Lotan R, Steller H, Larisch S (2004) The mitochondrial ARTS protein promotes apoptosis through targeting XIAP. *EMBO J* **23:** 1627–1635
Harbury PB, Zhang T, Kim PS, Alber T (1993) A switch between two-, three-, and four-stranded coiled coils in GCN4 leucine zipper mutants. *Science* **262:** 1401–1407
Honnappa S, John CM, Kostrewa D, Winkler FK, Steinmetz MO (2005) Structural insights into the EB1-APC interaction. *EMBO J* **24:** 261–269
Hsu SC, Hazuka CD, Roth R, Foletti DL, Heuser J, Scheller RH (1998) Subunit composition, protein interactions, and structures of the mammalian brain sec6/8 complex and septin filaments. *Neuron* **20:** 1111–1122
Joo E, Tsang CW, Trimble WS (2005) Septins: traffic control at the cytokinesis intersection. *Traffic* **6:** 626–634
Kinoshita M (2003) The septins. *Genome Biol* **4:** 236
Kinoshita M, Field CM, Coughlin ML, Straight AF, Mitchison TJ (2002) Self- and actin-templated assembly of Mammalian septins. *Dev Cell* **3:** 791–802
Kozubowski L, Larson JR, Tatchell K (2005) Role of the septin ring in the asymmetric localization of proteins at the mother-bud neck in *Saccharomyces cerevisiae*. *Mol Biol Cell* **16:** 3455–3466
Kozubowski L, Panek H, Rosenthal A, Bloecher A, DeMarini DJ, Tatchell K (2003) A Bni4-Glc7 phosphatase complex that recruits chitin synthase to the site of bud emergence. *Mol Biol Cell* **14:** 26–39
Kusch J, Meyer A, Snyder MP, Barral Y (2002) Microtubule capture by the cleavage apparatus is required for proper spindle positioning in yeast. *Genes Dev* **16:** 1627–1639
Larisch S, Yi Y, Lotan R, Kerner H, Eimerl S, Tony Parks W, Gottfried Y, Birkey Reffey S, de Caestecker MP, Danielpour D, Book-Melamed N, Timberg R, Duckett CS, Lechleider RJ, Steller H, Orly J, Kim SJ, Roberts AB (2000) A novel mitochondrial septin-like protein, ARTS, mediates apoptosis dependent on its P-loop motif. *Nat Cell Biol* **2:** 915–921
Liu Q, Li MZ, Liu D, Elledge SJ (2000) Rapid construction of recombinant DNA by the univector plasmid-fusion system. *Methods Enzymol* **328:** 530–549
Longtine MS, Bi E (2003) Regulation of septin organization and function in yeast. *Trends Cell Biol* **13:** 403–409
Low C, Macara IG (2006) Structural analysis of septin 2, 6, and 7 complexes. *J Biol Chem* **281:** 30697–30706
Mendoza M, Hyman AA, Glotzer M (2002) GTP binding induces filament assembly of a recombinant septin. *Curr Biol* **12:** 1858–1863
Nakagawa T, Cheng Y, Ramm E, Sheng M, Walz T (2005) Structure and different conformational states of native AMPA receptor complexes. *Nature* **433:** 545–549
Nguyen TQ, Sawa H, Okano H, White JG (2000) The *C. elegans* septin genes, unc-59 and unc-61, are required for normal post-embryonic cytokineses and morphogenesis but have no essential function in embryogenesis. *J Cell Sci* **113** (Part 21)**:** 3825–3837
Ohi M, Li Y, Cheng Y, Walz T (2004) Negative staining and image classification—powerful tools in modern electron microscopy. *Biol Proced Online* **6:** 23–34
Philipps B, Hennecke J, Glockshuber R (2003) FRET-based *in vivo* screening for protein folding and increased protein stability. *J Mol Biol* **327:** 239–249
Reinsch S, Karsenti E (1994) Orientation of spindle axis and distribution of plasma membrane proteins during cell division in polarized MDCKII cells. *J Cell Biol* **126:** 1509–1526
Russell SE, Hall PA (2005) Do septins have a role in cancer? *Br J Cancer* **93:** 499–503
Schmidt K, Nichols BJ (2004) A barrier to lateral diffusion in the cleavage furrow of dividing mammalian cells. *Curr Biol* **14:** 1002–1006
Sheffield PJ, Oliver CJ, Kremer BE, Sheng S, Shao Z, Macara IG (2003) Borg/septin interactions and the assembly of mammalian septin heterodimers, trimers, and filaments. *J Biol Chem* **278:** 3483–3488
Spiliotis ET, Kinoshita M, Nelson WJ (2005) A mitotic septin scaffold required for Mammalian chromosome congression and segregation. *Science* **307:** 1781–1785
Steinmetz MO, Stock A, Schulthess T, Landwehr R, Lustig A, Faix J, Gerisch G, Aebi U, Kammerer RA (1998) A distinct 14 residue site triggers coiled-coil formation in cortexillin I. *EMBO J* **17:** 1883–1891
Suter M, Riek U, Tuerk R, Schlattner U, Wallimann T, Neumann D (2006) Dissecting the role of 5′-AMP for allosteric stimulation, activation, and deactivation of AMP-activated protein kinase. *J Biol Chem* **281:** 32207–32216
Takizawa PA, DeRisi JL, Wilhelm JE, Vale RD (2000) Plasma membrane compartmentalization in yeast by messenger RNA transport and a septin diffusion barrier. *Science* **290:** 341–344
Tucker J, Sczakiel G, Feuerstein J, John J, Goody RS, Wittinghofer A (1986) Expression of p21 proteins in *Escherichia coli* and stereochemistry of the nucleotide-binding site. *EMBO J* **5:** 1351–1358
Versele M, Gullbrand B, Shulewitz MJ, Cid VJ, Bahmanyar S, Chen RE, Barth P, Alber T, Thorner J (2004) Protein–protein interactions governing septin heteropentamer assembly and septin filament organization in *Saccharomyces cerevisiae*. *Mol Biol Cell* **15:** 4568–4583
Versele M, Thorner J (2004) Septin collar formation in budding yeast requires GTP binding and direct phosphorylation by the PAK, Cla4. *J Cell Biol* **164:** 701–715
Versele M, Thorner J (2005) Some assembly required: yeast septins provide the instruction manual. *Trends Cell Biol* **15:** 414–424
Vrabioiu AM, Gerber SA, Gygi SP, Field CM, Mitchison TJ (2004) The majority of the *Saccharomyces cerevisiae* septin complexes do not exchange guanine nucleotides. *J Biol Chem* **279:** 3111–3118
Zhang J, Kong C, Xie H, McPherson PS, Grinstein S, Trimble WS (1999) Phosphatidylinositol polyphosphate binding to the mammalian septin H5 is modulated by GTP. *Curr Biol* **9:** 1458–1467